Prognostic Utility of ^{90}Y Radioembolization Dosimetry Based on Fusion ^{99m}Tc-Macroaggregated Albumin–^{99m}Tc-Sulfur Colloid SPECT

Marnix G.E.H. Lam[1,2], Michael L. Goris[3], Andrei H. Iagaru[3], Erik S. Mittra[3], John D. Louie[1], and Daniel Y. Sze[1]

[1]Division of Interventional Radiology, Stanford University School of Medicine, Stanford, California; [2]Department of Radiology and Nuclear Medicine, UMC Utrecht, Utrecht, The Netherlands; and [3]Division of Nuclear Medicine and Molecular Imaging, Stanford University School of Medicine, Stanford, California

Planning hepatic ^{90}Y radioembolization activity requires balancing toxicity with efficacy. We developed a dual-tracer SPECT fusion imaging protocol that merges data on radioactivity distribution with physiologic liver mapping. **Methods:** Twenty-five patients with colorectal carcinoma and bilobar liver metastases received whole-liver radioembolization with resin microspheres prescribed as per convention (mean administered activity, 1.69 GBq). As part of standard treatment planning, all patients underwent SPECT imaging after intraarterial injection of 37 MBq of ^{99m}Tc-macroaggregated albumin (^{99m}Tc-MAA) to simulate subsequent ^{90}Y distribution. Immediately afterward, patients received 185 MBq of labeled sulfur colloid (^{99m}Tc-SC) intravenously as a biomarker for normal hepatic reticuloendothelial function and SPECT was repeated. The SPECT images were coregistered and fused. A region-based method was used to predict the ^{90}Y radiation absorbed dose to functional liver tissue (D_{FL}) by calculation of ^{99m}Tc-MAA activity in regions with ^{99m}Tc-SC uptake. Similarly, the absorbed dose to tumor (D_T) was predicted by calculation of ^{99m}Tc-MAA activity in voxels without ^{99m}Tc-SC uptake. Laboratory data and radiographic response were measured for 3 mo, and the survival of patients was recorded. SPECT-based D_T and D_{FL} were correlated with parameters of toxicity and efficacy. **Results:** Toxicity, as measured by increase in serum liver enzymes, correlated significantly with SPECT-based calculation of D_{FL} at all time points ($P < 0.05$) (mean D_{FL}, 27.9 Gy). Broad biochemical toxicity (>50% increase in all liver enzymes) occurred at a D_{FL} of 24.5 Gy and above. In addition, in uni- and multivariate analysis, SPECT-based calculation of D_T (mean D_T, 44.2 Gy) correlated with radiographic response ($P < 0.001$), decrease in serum carcinoembryonic antigen ($P < 0.05$), and overall survival ($P < 0.01$). The cutoff value of D_T for prediction of 1-y survival was 55 Gy (area under the receiver-operating-characteristic curve = 0.86; $P < 0.01$). Patients who received a D_T of more than 55 Gy had a median survival of 32.8 mo, compared with 7.2 mo in patients who received less ($P < 0.05$). **Conclusion:** Dual-tracer ^{99m}Tc-MAA–^{99m}Tc-SC fusion SPECT offers a physiology-based imaging tool with significant prognostic power that may lead to improved personalized activity planning.

Key Words: radioembolization; hepatic metastases; colorectal carcinoma; dosimetry; treatment planning

J Nucl Med 2013; 54:2055–2061
DOI: 10.2967/jnumed.113.123257

Yttrium-90 radioembolization is a rapidly emerging radionuclide treatment modality for hepatic malignancy that improves progression-free and overall survival in appropriate patients (*1–4*). Activity planning aims to maximize the effect of treatment while keeping toxicity acceptably low. However, the current activity calculation methods are based on empiric data with regard to both efficacy and safety, without established dose–response relationships (*5*). Resin microsphere activity is calculated on the basis of body surface area (BSA) and fractional liver involvement, whereas glass microsphere activity is calculated on the basis of a whole-liver partition model derived from the MIRD equations for dose calculation (*6*). Neither accounts for the heterogeneous intrahepatic microsphere distribution and the resultant differential radiation absorbed dose in tumors and normal liver tissue.

A potential approach to better customization of activity is anatomic partition modeling (*7–9*). The involved liver may be segmented into 2 compartments, and the desired activity is calculated on the basis of intercompartmental volumes and activity ratios. Because compartmental boundaries are drawn on the basis of anatomic images, these methods are time-consuming and subject to considerable error in tumor delineation. Partition modeling in its present capacity is therefore advised only for patients with a limited number of large, hypervascular tumors (*10*). In most patients with liver metastases, however, disease is diffusely distributed throughout the liver, includes multiple tumors that are difficult to delineate, and therefore is not amenable to anatomic partition modeling (*5,10*).

We introduce a physiology-based segmentation tool that uses a dual-tracer SPECT technique combining ^{99m}Tc-macroaggregated albumin (^{99m}Tc-MAA) SPECT for simulation of ^{90}Y activity distribution and ^{99m}Tc-sulfur colloid (^{99m}Tc-SC) SPECT for evaluation of functional liver parenchyma (reticuloendothelial function). We aimed to validate the utility of this method by correlating its results with efficacy and toxicity in patients treated with whole-liver radioembolization.

MATERIALS AND METHODS

Patient Selection

The study included 25 patients from January 2007 to January 2011 who had multiple unresectable liver metastases from colorectal carcinoma

Received Mar. 16, 2013; revision accepted Jun. 26, 2013.
For correspondence or reprints contact: Daniel Y. Sze, Division of Interventional Radiology, Stanford University School of Medicine, 300 Pasteur Dr., Stanford, CA 94305-5642.
E-mail: dansze@stanford.edu
Published online Oct. 21, 2013.

and received whole-liver treatment with resin microspheres in a single session. There were 10 men and 15 women, of mean and median age 58 y (range, 25–80 y). All patients had liver-dominant disease for which hepatic metastases were considered to be the most longevity-threatening component. Exclusion criteria included mismatch between ^{99m}Tc-MAA and subsequent ^{90}Y-microsphere injection site, imaging failure (SPECT not performed, injection failure), and staged treatment in 2 separate sessions. Clinical data of the studied population are summarized in Table 1. All patients underwent combined ^{99m}Tc-MAA–^{99m}Tc-SC SPECT imaging as part of their diagnostic work-up. Data were handled in accordance with the Health Insurance Portability and Accountability Act. The institutional review board approved this study, and the requirement to obtain informed consent was waived.

Radioembolization

Activity calculations and treatments were performed according to international consensus guidelines (*11–13*). All patients were treated with resin microspheres (SIR-Spheres; SirTex Inc.). The prescribed activity was calculated on the basis of BSA and tumor liver involvement (LI), defined as a fraction of the total liver parenchyma (*14*):

$$\text{Prescribed activity (GBq)} = \text{BSA}\left(\text{m}^2\right) - 0.2 + \text{LI}. \qquad \text{Eq. 1}$$

Significant hepatopulmonary shunting was compensated for by the recommended activity adjustment (*13*).

Pretreatment V-Vial (Wheaton Industries, Inc.) activity and post-treatment V-Vial, tubing, and catheter activity were measured in a leak-proof Nalgene (Thermo Fisher Scientific) container using a MicroRem meter (Thermo Scientific/Bicron) at a set standard geometry. Measurements were processed by calibrated conversion algorithms (SirTex Inc.) to calculate the percentage of residual activity. The hepatic administered activity (A) was determined by correcting the prepared activity for residual activity and for the fractional lung shunt (LS).

$$\text{A} = (\text{prescribed dose} - \text{residual activity}) \times (1 - \text{LS}). \qquad \text{Eq. 2}$$

Clinical and laboratory follow-up was performed 2, 4, 8, and 12 wk after treatment and at intervals prescribed by the medical oncologist thereafter. Follow-up contrast-enhanced CT at 3 mo was used to analyze objective response according to Response Evaluation Criteria in Solid Tumors (RECIST 1.1). PET scans were not generally available for review. One masked author performed over-reads of all clinical film interpretations.

TABLE 1
Demographics, Baseline Characteristics, and Oncologic Histories of Cohort

Characteristic	Data*
Sex, male/female	10/15
Age (y)	58 (25–80)
Previous systemic treatment	
Chemotherapy	24
Antiangiogenic agents	23
Anti-EGFR agents	13
Previous liver-directed treatment	
Partial liver resection	9
Radiofrequency ablation	8
External-beam radiotherapy†	1
ECOG performance status	
0	17
1	8
Extrahepatic disease	
Pulmonary metastases	13
Lymph node metastases	6
Total	15
Baseline laboratory values	
WBC count (10^9/L)	7.4 (3.4–12)
Platelet count (10^9/L)	265 (94–466)
Hemoglobin (g/dL)	12.4 (9.7–15)
Serum AST (IU/L)	37 (11–116)
Serum ALT (IU/L)	39 (13–99)
Serum total bilirubin (mg/dL)	0.5 (0.1–1.7)
Serum alkaline phosphatase (IU/L)	138 (64–713)
Serum albumin (g/dL)	3.5 (2.6–4)
Carcinoembryonic antigen (ng/mL)	33 (1.3–2,213)
Liver tumor involvement (%)	25 (5–60)
BSA (m^2)	1.88 (1.37–2.31)
Calculated prescribed activity (GBq)	1.85 (1.07–2.68)
Calculated lung shunt (%)	6.6 (0–13.8)
Administered activity (GBq)	1.69 (0.97–2.33)
Liver weight (g)	1,826 (941–2,958)
Whole-liver absorbed dose (D_{WL}) (Gy)	48.8 (29.8–68.5)

*Qualitative data are expressed as numbers; continuous data are expressed as median and range.

†Patient received preoperative chemoradiotherapy for local recurrence of rectal carcinoma. Mean radiation absorbed dose to liver was 4.7 Gy as determined by dose–volume histogram analysis.

ECOG = Eastern Cooperative Oncology Group.

Imaging Procedures

At the time of the preparatory angiography session and after endovascular skeletonization of the hepatic artery, ^{99m}Tc-MAA (37 MBq) was administered intraarterially to simulate the planned treatment with ^{90}Y-microspheres. Activity lower than the standard 150 MBq was used to facilitate combined ^{99m}Tc-MAA–^{99m}Tc-SC SPECT imaging.

Whole-body planar scintigraphy and hepatic SPECT imaging were performed within 1 h after tracer administration to calculate the lung shunt fraction, to exclude any extrahepatic deposition, and to depict intrahepatic radiopharmaceutical distribution. Immediately after the first SPECT scan, without moving the patient in the scanner to optimize image fusion, an excess of ^{99m}Tc-SC (185 MBq) was injected intravenously and SPECT imaging was repeated after a 5-min delay.

SPECT data were acquired on a dual-head Infinia Hawkeye 4 γ camera (GE Healthcare). SPECT images were acquired on a 64 × 64 matrix (voxel size, 0.884 mm^3) using a 130- to 150-keV energy window and a low-energy high-resolution collimator. All SPECT data were acquired in 120 projections (15 s per projection) over a 360° full circular orbit.

Image Processing and Analysis

Data were reconstructed by applying filtered backprojection and a Butterworth postreconstruction filter (Fc, 0.23; order, 6), using Segami software (Segami Corp.). For each patient, corrected ^{99m}Tc-SC images were constructed by subtracting ^{99m}Tc-MAA images (first SPECT) from the combined ^{99m}Tc-MAA–^{99m}Tc-SC images (second SPECT). Voxels positive for ^{99m}Tc-SC were assigned to the functional-liver compartment, whereas voxels negative for ^{99m}Tc-SC but positive for ^{99m}Tc-MAA were assigned to the tumor compartment. Next, a map of functional liver was produced by applying a threshold that identified all voxels with 10% or more of the maximum ^{99m}Tc-SC uptake per voxel, using software programmed in IDL 6.1 (Research Systems,

Inc.). Similarly, a tumor map was generated from the ^{99m}Tc-MAA images by applying the 10% threshold to the ^{99m}Tc-MAA images and excluding all voxels with ^{99m}Tc-SC uptake (Figs. 1 and 2). On the basis of these maps, tumor and functional-liver regions of interest (ROI_T and ROI_{FL}) were defined as all voxels negative for ^{99m}Tc-SC but positive for ^{99m}Tc-MAA (ROI_T) and as all voxels positive for ^{99m}Tc-SC (ROI_{FL}). Partition was based solely on these physiologic parameters with no need for anatomic delineation and its inherent error. For comparison, alternative thresholds of 5% and 20% were also evaluated.

ROI volume and ^{99m}Tc-MAA activity in each ROI were translated to a radiation absorbed dose using A (GBq), the ROI volume in liters, and an estimated density of all hepatic tissue of 1.029 kg/L (based on the specific density of soft tissue in general). The mean radiation absorbed dose to tumor (D_T) was thus calculated, derived from the MIRD equations for dose calculation (*6*):

$$D_T = (\text{MAA activity } ROI_T/\text{total MAA activity}) \times A \times 1.029^{-1} \times \text{volume } ROI_T^{-1} \times 50, \quad \text{Eq. 3}$$

where MAA activity ROI_T is the ^{99m}Tc-MAA activity in ROI_T (i.e., tumor tissue as defined by ^{99m}Tc-MAA uptake threshold), total MAA activity is the administered ^{99m}Tc-MAA activity corrected for the lung shunt, A is the administered ^{90}Y activity in GBq, 1.029^{-1} is the density conversion factor for hepatic tissue, volume ROI_T is the volume of ROI_T in liters, and 50 is the conversion factor for ^{90}Y from GBq/kg to Gy derived from MIRD (*6*).

Similarly, the mean D_{FL} was calculated as

$$D_{FL} = (\text{MAA activity } ROI_{FL}/\text{total MAA activity}) \times A \times 1.029^{-1} \times \text{volume } ROI_{FL}^{-1} \times 50, \quad \text{Eq. 4}$$

where MAA activity ROI_{FL} is the ^{99m}Tc-MAA activity in ROI_{FL} (i.e., normal liver as defined by ^{99m}Tc-SC uptake threshold), total MAA activity is the administered ^{99m}Tc-MAA activity corrected for the lung shunt, and volume ROI_{FL} is the volume of ROI_{FL} in liters.

For comparison, the mean whole-liver radiation absorbed dose (D_{WL}) was calculated using conventional MIRD formulae, assuming homogeneous distribution and absorption of all the administered activity and energy in the liver:

$$D_{WL} = A \times 1.029^{-1} \times \text{volume}_{WL}^{-1} \times 50, \quad \text{Eq. 5}$$

where volume_{WL} is the volume of the whole liver in liters, calculated from preprocedural CT scans.

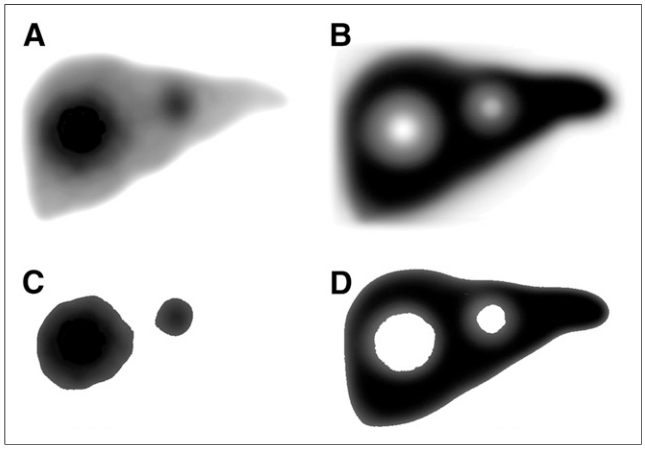

FIGURE 1. Schematic representation of physiologic partition model of liver. (A and B) Maximum-intensity projection of ^{99m}Tc-MAA SPECT (A) and ^{99m}Tc-SC SPECT MIP (B), showing concentrated uptake of ^{99m}Tc-MAA in and around 2 tumors and relative photopenia in these areas on ^{99m}Tc-SC image. (C) Tumor map contains only those voxels positive for ^{99m}Tc-MAA uptake and negative for ^{99m}Tc-SC uptake. (D) Functional liver map contains all voxels positive for ^{99m}Tc-SC uptake. Because of spill-over and partial-volume effects, threshold function was used to define voxels as positive for ^{99m}Tc-MAA or ^{99m}Tc-SC uptake.

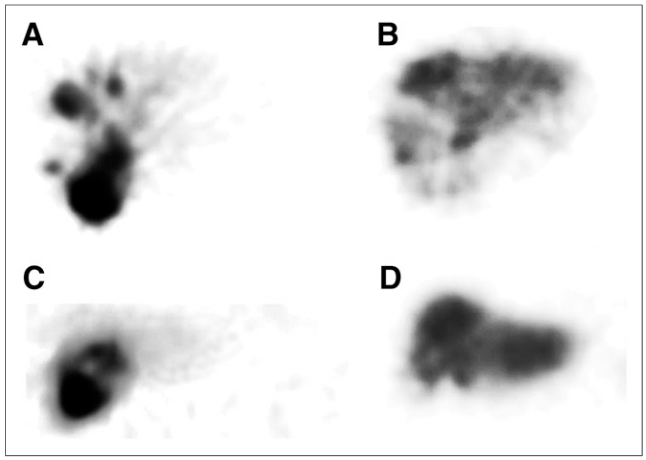

FIGURE 2. Physiologic partition model of liver. (A and B) Transaxial slices (thick slab) of ^{99m}Tc-MAA SPECT (A) and ^{99m}Tc-SC SPECT (B), showing concentrated uptake of ^{99m}Tc-MAA in and around physiologic tumor tissue in right lobe and relative photopenia in these areas on ^{99m}Tc-SC image. (C and D) Coronal reformats of ^{99m}Tc-MAA SPECT (C) and ^{99m}Tc-SC SPECT (D) confirm this yin-yang phenomenon.

Statistical Analysis

A commercial software package was used for statistical analysis (SPSS for Windows, version 19.0; SPSS Inc.). All continuous variables were tested for normal distribution probability using Kolmogorov–Smirnov tests, including normality plots. Median and range were reported for non–normally distributed variables, mean and range for normally distributed variables. For individual correlation of 2 continuous variables, the Pearson or Spearman correlation coefficient was used, depending on normality. Survival analysis was performed using Kaplan–Meier curves with the log rank test for comparison. Receiver-operating-characteristic analysis was used to determine cutoff values for clinical use of the presented parameters. A P value of less than 0.05 was considered statistically significant.

RESULTS

The patients selected were heavily pretreated, with almost all (92%) having received systemic chemotherapy and bevacizumab (Table 1). Half the patients (52%) also received epidermal growth factor receptor antagonists, and almost half (48%) had undergone liver-directed treatments including resection, ablation, embolization, and external-beam radiotherapy. All patients maintained a good performance status (Eastern Cooperative Oncology Group scores of 0–1) and baseline laboratory values within acceptable ranges. All patients had multiple metastases in both liver lobes, with a median estimated tumor involvement of the liver of 25% (range, 5%–60%). All were treated with resin microspheres with whole-liver treatment in a single session. Mean A was 1.69 GBq (range, 0.97–2.33 GBq), and mean D_{WL} was 48.8 Gy (range, 29.8–68.5 Gy). Only 3 patients restarted systemic treatment within our 3-mo follow-up period after radioembolization (irinotecan plus bevacizumab after 2 mo, cetuximab after 2 mo, and oxaliplatin plus

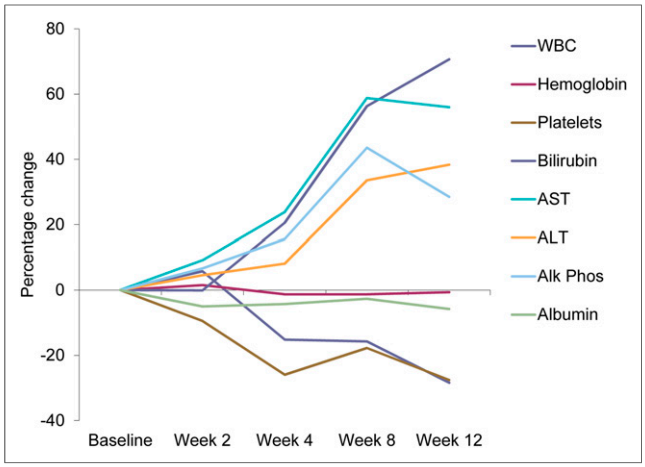

FIGURE 3. Hematologic and serum chemistry changes from baseline and 2, 4, 8, and 12 wk after radioembolization, expressed as mean percentage change. WBC = white blood cell count; bilirubin = total serum bilirubin; alk phos = alkaline phosphatase.

5-fluorouracil after 1.5 wk). At least 4 other patients restarted some form of systemic treatment beyond 3 mo.

With a 10% threshold, where any voxel with at least 10% of the maximum ^{99m}Tc-MAA or ^{99m}Tc-SC activity was considered positive for that marker, the mean D_{FL} was 27.9 Gy (range, 11.9–41.6). The changes in liver function tests (serum bilirubin, aspartate aminotransferase [AST], alanine transaminase [ALT], alkaline phosphatase, and albumin) and blood counts (white blood cell count, hemoglobin, and platelets) during the first 3 mo after radioembolization are depicted in Figure 3. Significant correlations were found between D_{FL} and changes in serum liver enzymes (AST, ALT, and alkaline phosphatase) at virtually all time points ($r = 0.38$–0.69; $P < 0.01$). Only weaker trends were found between D_{FL} and blood counts, bilirubin, and albumin. Comparing laboratory values with D_{WL} instead of D_{FL} yielded a similar but weaker pattern of correlations, with only a few reaching statistical significance (AST in weeks 4–8 and ALT in week 2–8).

According to the National Cancer Institute's Common Terminology Criteria for Adverse Events, version 4.02, these changes in laboratory values were classifiable as mild toxicity in most patients (Table 2). A significant correlation was found between the cumulative toxicity grades and D_{FL} ($r = 0.48$; $P < 0.01$) (Fig. 4) and D_{WL} ($r = 0.44$; $P < 0.05$). Toxicity grades were most pronounced for the liver enzymes AST, ALT, and alkaline phosphatase. Total bilirubin levels increased but reached thresholds of toxicity in only a few patients, whereas minor decreases in albumin levels were classified as toxicity in most patients because of low pretreatment levels already near the toxicity threshold (Table 2; Fig. 3). Broad biochemical toxicity, defined as a 50% increase in each of the 3 measured liver enzymes, occurred in 9 of 25 patients (36%). Receiver-operating-curve analysis revealed a good predictive value of D_{FL} to predict this composite toxicity, with an area under the curve of 0.88 ($P < 0.01$; 95% confidence interval, 0.66–0.99). All cases of a 50% increase in all 3 liver enzymes occurred at a D_{FL} of 24.5 Gy and above.

TABLE 2
Toxicity after Radioembolization According to National Cancer Institute's Common Terminology Criteria for Adverse Events, Version 4.02

Patient	WBC	Hemoglobin	Platelets	Bilirubin	AST	ALT	Alk Phos	Albumin
1					1	1		1
2			1		1		1	1
3					1	1		2
4		1			1			1
5								2
6	1			1			1	1
7					1		1	
8			3		1	1	1	1
9	1				1		1	
10								
11					1			2
12		2	1	2	1			2
13								2
14		1	1		1	1	1	1
15	2							
16								
17							1	1
18					1	1	1	
19								
20								
21								2
22		1	1					2
23			2	2				
24	3	2						
25					1			

WBC = white blood cell count; alk phos = alkaline phosphatase.

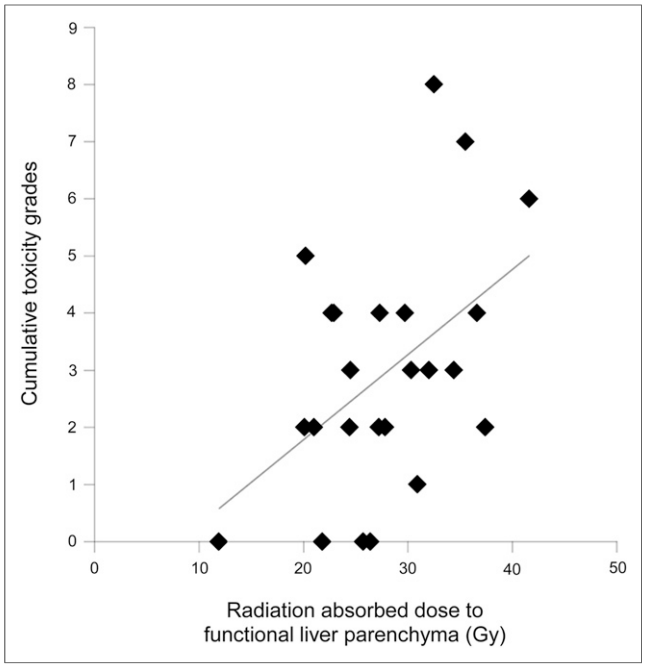

FIGURE 4. D_{FL} in grays on *x*-axis vs. cumulative toxicity in grades according to National Cancer Institute's Common Terminology Criteria for Adverse Events, version 4.02. $r = 0.48$ ($P < 0.01$).

Using the 10% threshold, the mean D_T was 44.2 Gy (range, 11.3–105.7 Gy). Response rate according to RECIST 1.1 was only 26.7%, with no complete responders (stable disease, 60.0%; disease control, 86.7%; progressive disease, 13.3%). Responders received a D_T (mean ± SD) of 82.7 ± 23.9 Gy, versus 31.0 ± 10.9 Gy for nonresponders ($P < 0.001$). Responders versus nonresponders received 1.76 ± 0.26 GBq and 1.68 ± 0.43 GBq, respectively ($P = 0.74$), and a D_{WL} of 49.1 ± 6.3 Gy and 52.8 ± 11.0 Gy, respectively ($P = 0.54$), indicating that only differences in intrahepatic distribution of the dose and not the total liver dose impacted efficacy. Median liver tumor involvement was 25% for both the responders and the nonresponders ($P = 0.98$).

CEA levels showed a median decrease of 28.8% (range, −84.2 to +329.5%) at week 2, 50% (range, −94.7 to +329.5%) at week 4, and 31.3% (range, −94.7 to +430.3%) at week 8. These changes correlated with D_T at week 4 ($r = -0.45$; $P < 0.05$) and at week 8 ($r = -0.43$; $P < 0.05$). Correlation was found for D_{WL} only at week 8 ($r = -0.53$; $P < 0.05$).

Median follow-up after radioembolization was 40.8 mo (range, 20–67.7 mo). At the time of writing, 5 patients were still alive and 1 patient had been lost to follow-up after 9.7 mo. Median overall survival was 10.8 mo. D_T proved to be the only predictor of survival ($P < 0.01$). No other correlations were found between survival and clinical, laboratory, or procedural parameters, including D_{WL} ($P = 0.23$), previous systemic ($P = 0.20$) and liver-directed treatments ($P = 0.57$), liver tumor involvement ($P = 0.79$), extrahepatic disease ($P = 0.87$), and performance status ($P = 0.70$).

The 1- and 2-y survival rates were 45.8% and 25.0%, respectively. Receiver-operating-curve analysis of D_T versus 1- and 2-y survival led to an area under the curve of 0.86 ($P < 0.01$; 95% confidence interval, 0.71–1.0) and 0.82 ($P < 0.05$; 95% confidence interval, 0.58–1.0), respectively (Fig. 5). The 1-y survival for patients who received a D_T of more than 55 Gy was 100%, whereas the 1-y survival for patients who received less than 55 Gy was 24%. Similarly, the 2-y survival for patients who received a D_T of more than 77 Gy was 100%, whereas the 2-y survival for patients who received less than 77 Gy was 10%. The median survival of patients who received a D_T of more than 55 Gy was 32.8 mo, whereas patients who received less than 55 Gy had a median survival of only 7.2 mo ($P < 0.05$) (Fig. 6).

The impact of applying different thresholds to define positive ^{99m}Tc-MAA and ^{99m}Tc-SC uptake was studied, using 5%, 10%, and 20% of the maximum activity per voxel as thresholds (Table 3). A higher threshold resulted in higher calculated D_T and D_{FL} ($P < 0.01$). This was the result of smaller ROIs and higher activity per voxel caused by the higher thresholds. This increase was more pronounced for D_T. The ratio of tumor uptake (D_T) to functional liver uptake (D_{FL}) showed an increase from a mean of 1.2 at a 5% threshold to 1.8 at a 10% threshold to 4.2 at a 20% threshold. The predictive power for toxicity, response, and survival was not significantly influenced by different thresholding. Data and statistics were thus reported at the 10% level to balance prognostic power for efficacy and for toxicity.

DISCUSSION

Activity planning for radioembolization remains inexact and unscientific, likely contributing to the rate of nonresponse, which can be up to 80% (*1*), and to hepatotoxicity, which can occur in up to 20% of patients (*15,16*). The liver, despite its qualities of dual blood supply, regeneration, and redundancy, is highly radiosensitive. Absorbed doses high enough to be tumoricidal usually exceed the maximum tolerated absorbed dose for the background liver, limiting the application of radiation therapy to hepatic malignancies (*17*). The inhomogeneous distribution of intraarterially administered radioembolization microspheres can overcome this limitation by delivering the highest absorbed doses to hypervascular, arterially supplied tumors, while limiting deposition in the portal vein–supplied functional liver. However, a reproducible method to predict or to measure the actual absorbed dose to tumor and to functional liver remains elusive.

By the earliest activity planning method, or empiric method, patients were treated with a predetermined activity that reflected

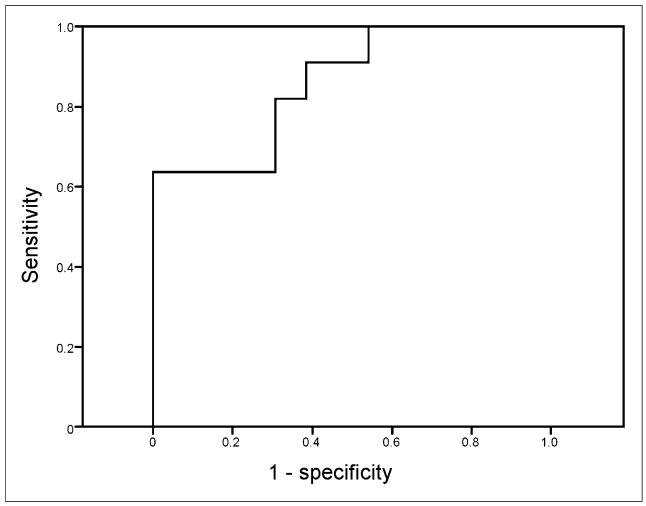

FIGURE 5. Receiver-operator-characteristic curve for prediction of 1-y survival after radioembolization by D_T. At tumor dose of at least 55 Gy, all patients survived at least 1 y. Area under curve = 0.86 ($P < 0.01$; 95% confidence interval, 0.71–1.0).

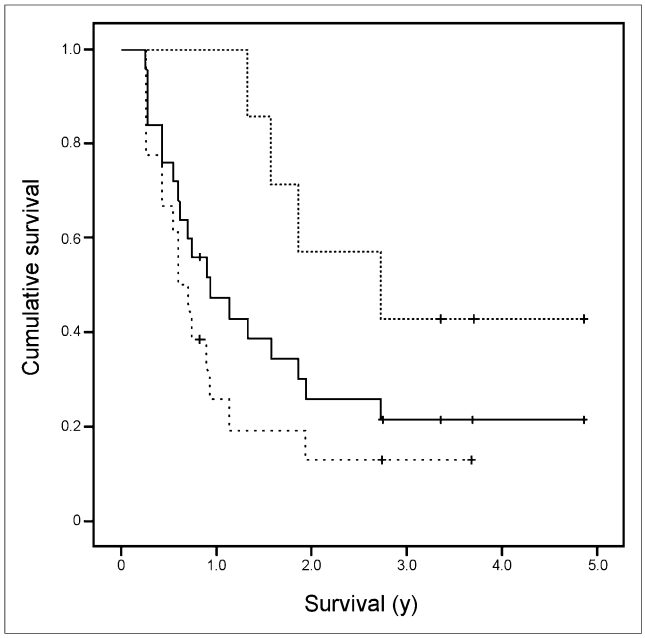

FIGURE 6. Kaplan–Meier curves for patients treated with D_T of more than 55 Gy (upper dashed line) vs. less than 55 Gy (lower dashed line), with median survivals of 32.8 mo vs. 7.2 mo ($P < 0.05$). Survival of total population is depicted as solid line (median, 10.8 mo).

only tumor liver involvement. Tumor involvement that was less than 25%, 25%–50%, or more than 50% of the total liver volume was treated with 2, 2.5, or 3 GBq, respectively (*18*). It was eventually recognized that this method led to an unacceptable incidence of hepatotoxicity due to radioembolization-induced liver disease (*14*). The empiric method was supplanted by the current BSA method, which has become adopted as the standard for resin microspheres. This change led to a lower incidence of radioembolization-induced liver disease, not so much because of more accurate dosimetry as because administered activity was significantly reduced (*15*). The BSA method was proposed without scientific derivation and, although relatively safe, results in potentially subtherapeutic doses in patients with enlarged livers (*19*).

The standard activity planning method for glass microspheres is a MIRD-based calculation that considers the weight of the treated tissue and a target absorbed dose averaged over the entire treatment volume, sometimes erroneously termed the partition method. This method, as currently practiced, uses a nonpartitioned 1-compartment model of uniform distribution to perform the calculations (target, 80–120 Gy) but assumes a large degree of nonuniform distribution to maintain a background functional liver dose of less than 30 Gy and, thus, tolerable hepatotoxicity. The actual degree of nonuniformity is not typically quantified.

TABLE 3
Influence of Threshold on Dosimetry Parameters

Parameter	5% threshold	10% threshold	20% threshold
D_T in Gy	30.5 (5.1–86.7)	44.2 (11.3–105.7)	84.5 (23.3–259.4)
D_{FL} in Gy	26.0 (16.0–37.1)	27.9 (11.9–41.6)	30.7 (4.0–52.1)
D_T:D_{FL} ratio	1.2 (0.2–5.4)	1.8 (0.4–8.9)	4.2 (0.6–40.9)

Mean and range are reported. D_T:D_{FL} ratio is estimate of tumor-to-nontumor ratio.

Several groups have proposed improved partition method dosimetry based on quantitative ^{99m}Tc-MAA SPECT/CT (*7–9*). A study on 36 patients with 58 lesions of hepatocellular carcinoma treated with glass microspheres found that quantitative ^{99m}Tc-MAA SPECT/CT had a predictive value for response to radioembolization and survival (*8*). The accuracy in predicting the response of an individual lesion at 3 mo was 91%. Three false-positives were encountered in cases involving large, heterogeneous, partially necrotic lesions. This modified partition method has clear advantages over existing methods with regard to tumor dosimetry but has several important limitations: normal-liver tissue dosimetry and toxicity are not addressed; morphologic imaging–based tumor segmentation is limited by tumor number, heterogeneity, necrosis, and infiltrative spread; and the method is operator-dependent and labor- and time-intensive (*19*). This partition method is most useful in patients with few and sharply delineated tumors. Unfortunately, such patients are only a small subpopulation of those treated by radioembolization.

Our method of using combined ^{99m}Tc-MAA–^{99m}Tc-SC SPECT imaging offers a physiologic imaging tool that overcomes the limitations of morphologic imaging–based partition modeling. Absorbed dose to both tumor and functional liver is addressed, yielding good prognostic power with regard to both efficacy and toxicity. Tissue segmentation is based purely on physiology, relying on 2 standard nuclear medicine procedures, post–intraarterial ^{99m}Tc-MAA scintigraphy and post–intravenous ^{99m}Tc-SC scintigraphy (*20*), obviating manual morphology-based tumor segmentation. Multiplicity, size, distribution, heterogeneity, necrosis, and infiltrative growth of tumors are inherently accommodated. Our method is fully automated and fast and can be operator-independent.

Several limitations of our method remain and are the subject of further refinement. One limitation is that the uptake of ^{99m}Tc-SC identifies regions of intact reticuloendothelial function, which may or may not coincide perfectly with regions of intact hepatocellular function. The method currently averages all voxels in the ROIs and does not calculate the absorbed dose for individual lesions, which can vary. The calculated absorbed dose is an estimation influenced by partial-volume and spillover effects. Adjustment of the quantification thresholds can partially overcome this problem but can result in large differences in calculated D_T across the range of potential thresholds. It remains unproven which threshold correlates best with anatomic tumor delineation, tumor volumes, and radiation absorbed doses. However, such correlations may be unnecessary, since our physiology-based method proved to have a robust predictive power for outcomes regardless of which threshold was chosen. Further improvements are to be expected by introducing dose-point kernel reconstruction algorithms, iterative reconstruction methods, dual-isotope protocols for optimized quantification and coregistration, and CT-based attenuation correction (using SPECT/CT).

The presented feasibility study included only a homogeneous group of 25 heavily pretreated patients with metastatic colorectal cancer, all of whom received whole-liver salvage radioembolization in a single session. However, interpatient differences still exist, and the benefits of improved dosimetry (and possible confounding factors such as treatment history and disease burden) need to be

translated to larger cohorts. These preliminary results will also need to be translated to prospective clinical practice. Even though β irradiation has a biologic coefficient of 1.0 (equivalent to x-rays and γ-rays), the effect of prolonged exposure on a decay curve may be different from that of fractionated doses as given by external-beam radiation, and a D_{FL} of 30 Gy may or may not be a valid limit. A prospective dose-escalation study may be conducted to establish safety limits for D_{FL} and to further refine patient inclusion criteria and optimization of dose planning.

CONCLUSION

Fusion ^{99m}Tc-MAA–^{99m}Tc-SC SPECT imaging offers a true physiology-based imaging tool for outcome prediction after hepatic radioembolization. It offers a robust, reproducible, automated, and fast method, which demonstrates prognostic value and dose–response relationships for both toxicity and efficacy.

DISCLOSURE

The costs of publication of this article were defrayed in part by the payment of page charges. Therefore, and solely to indicate this fact, this article is hereby marked "advertisement" in accordance with 18 USC section 1734. Daniel Sze is on the medical or scientific advisory boards for Surefire Medical, Inc., Treus Medical, Inc., RadGuard Medical, Inc., and Jennerex Biotherapeutics, Inc.; is on the speaker's bureau for W.L. Gore, Inc.; and has provided clinical trial consultation for Sirtex, Inc., Nordion, Inc., and Biocompatibles, Inc. No other potential conflict of interest relevant to this article was reported.

REFERENCES

1. Coldwell D, Sangro B, Salem R, et al. Radioembolization in the treatment of unresectable liver tumors: experience across a range of primary cancers. *Am J Clin Oncol.* 2012;35:167–177.
2. Sangro B, Salem R, Kennedy A, et al. Radioembolization for hepatocellular carcinoma: a review of the evidence and treatment recommendations. *Am J Clin Oncol.* 2011;34:422–431.
3. Sangro B, Carpanese L, Cianni R, et al. Survival after yttrium-90 resin microsphere radioembolization of hepatocellular carcinoma across Barcelona clinic liver cancer stages: a European evaluation. *Hepatology.* 2011;54:868–878.
4. Vente MA, Wondergem M, van de Tweel I, et al. Yttrium-90 microsphere radioembolization for the treatment of liver malignancies: a structured meta-analysis. *Eur Radiol.* 2009;19:951–959.
5. Dezarn WA, Cessna JT, de Werd LA, et al. Recommendations of the American Association of Physicists in Medicine on dosimetry, imaging, and quality assurance procedures for ^{90}Y microsphere brachytherapy in the treatment of hepatic malignancies. *Med Phys.* 2011;38:4824–4845.
6. Gulec SA, Mesoloras G, Stabin M. Dosimetric techniques in ^{90}Y-microsphere therapy of liver cancer: the MIRD equations for dose calculations. *J Nucl Med.* 2006;47:1209–1211.
7. Kao YH, Hock Tan AE, Burgmans MC, et al. Image-guided personalized predictive dosimetry by artery-specific SPECT/CT partition modeling for safe and effective ^{90}Y radioembolization. *J Nucl Med.* 2012;53:559–566.
8. Garin E, Lenoir L, Rolland Y, et al. Dosimetry based on ^{99m}Tc-macroaggregated albumin SPECT/CT accurately predicts tumor response and survival in hepatocellular carcinoma patients treated with ^{90}Y-loaded glass microspheres: preliminary results. *J Nucl Med.* 2012;53:255–263.
9. Strigari L, Sciuto R, Rea S, et al. Efficacy and toxicity related to treatment of hepatocellular carcinoma with ^{90}Y-SIR spheres: radiobiologic considerations. *J Nucl Med.* 2010;51:1377–1385.
10. Lau WY, Kennedy AS, Kim YH, et al. Patient selection and activity planning guide for selective internal radiotherapy with yttrium-90 resin microspheres. *Int J Radiat Oncol Biol Phys.* 2012;82:401–407.
11. Coldwell D, Sangro B, Wasan H, et al. General selection criteria of patients for radioembolization of liver tumors: an international working group report. *Am J Clin Oncol.* 2011;34:337–341.
12. Lewandowski RJ, Sato KT, Atassi B, et al. Radioembolization with ^{90}Y microspheres: angiographic and technical considerations. *Cardiovasc Intervent Radiol.* 2007;30:571–592.
13. Kennedy A, Nag S, Salem R, et al. Recommendations for radioembolization of hepatic malignancies using yttrium-90 microsphere brachytherapy: a consensus panel report from the radioembolization brachytherapy oncology consortium. *Int J Radiat Oncol Biol Phys.* 2007;68:13–23.
14. Van Hazel G, Blackwell A, Anderson J, et al. Randomised phase 2 trial of SIR-Spheres plus fluorouracil/leucovorin chemotherapy versus fluorouracil/leucovorin chemotherapy alone in advanced colorectal cancer. *J Surg Oncol.* 2004;88:78–85.
15. Kennedy AS, McNeillie P, Dezarn WA, et al. Treatment parameters and outcome in 680 treatments of internal radiation with resin ^{90}Y-microspheres for unresectable hepatic tumors. *Int J Radiat Oncol Biol Phys.* 2009;74:1494–1500.
16. Sangro B, Gil-Alzugaray B, Rodriguez J, et al. Liver disease induced by radioembolization of liver tumors: description and possible risk factors. *Cancer.* 2008;112:1538–1546.
17. Lawrence TS, Robertson JM, Anscher MS, et al. Hepatic toxicity resulting from cancer treatment. *Int J Radiat Oncol Biol Phys.* 1995;31:1237–1248.
18. Gray B, van Hazel G, Hope M, et al. Randomised trial of SIR-Spheres plus chemotherapy vs. chemotherapy alone for treating patients with liver metastases from primary large bowel cancer. *Ann Oncol.* 2001;12:1711–1720.
19. Kao YH, Tan EH, Ng CE, et al. Clinical implications of the body surface area method versus partition model dosimetry for yttrium-90 radioembolization using resin microspheres: a technical review. *Ann Nucl Med.* 2011;25:455–461.
20. Rubin RA, Lichtenstein GR. Hepatic scintigraphy in the evaluation of solitary solid liver masses. *J Nucl Med.* 1993;34:697–705.

The Journal of NUCLEAR MEDICINE

Prognostic Utility of ^{90}Y Radioembolization Dosimetry Based on Fusion ^{99m}Tc-Macroaggregated Albumin–^{99m}Tc-Sulfur Colloid SPECT

Marnix G.E.H. Lam, Michael L. Goris, Andrei H. Iagaru, Erik S. Mittra, John D. Louie and Daniel Y. Sze

J Nucl Med. 2013;54:2055-2061.
Published online: October 21, 2013.
Doi: 10.2967/jnumed.113.123257

The Journal of Nuclear Medicine is published monthly.
SNMMI | Society of Nuclear Medicine and Molecular Imaging
1850 Samuel Morse Drive, Reston, VA 20190.
(Print ISSN: 0161-5505, Online ISSN: 2159-662X)

SNMMI SOCIETY OF NUCLEAR MEDICINE AND MOLECULAR IMAGING